Solar and Stellar Coronal Mass Ejections
Proceedings IAU Symposium No. 388, 2026
N. Gopalswamy, O. Malandraki, A. Vidotto & W. Manchester, eds.
doi:10.1017/S1743921324001790

High Time Resolution Heavy Ion Sensor Observations across a Collisionless Shock

B. L. Alterman[1,2], S. A. Livi[2,3], S. T. Lepri[3], J. M. Raines[3], R. M. Dewey[3], D. Trotta[5], S. A. Spitzer[4], C. M. Bert[2,3], L. M. Kistler[7], A. Galvin[7], G. Nicolaou[8], T. S. Horbury[5], Y. J. Rivera[6], C. J. Owen[8], D. Verscharen[8], J. Coburn[8], G. Lewis[8], R. A. D'Amicis[9], D. T. Carpenter[3], E. P. Shimoun[3], I. Gershkovich[3], K. Ploof[3], T. J. Eddy[3], A. Fedorov[10], D. Lario[2], H. Kucharek[7], K. Ogasawara[1], F. Allegrini[1], L. Ellis[7], P. Louran[10], T. Stubbs[2]

[1]NASA Goddard Space Flight Center
8800 Greenbelt Road
Greenbelt, MD 20771
USA

[2]Space Science
Southwest Research Institute
6220 Culebra Rd.
San Antonio, TX, 78238
USA

[3]Department of Climate and Space Sciences & Engineering
University of Michigan
Climate and Space Research Building
2455 Hayward St.
Ann Arbor, MI, 48109
USA

[4]Weizmann Institute of Science
234 Herzl Street
Rehovot 7610001
Israel

[5]The Blackett Laboratory
Department of Physics
Imperial College London
London SW7 2AZ
UK

[6]Center for Astrophysics | Harvard & Smithsonian
60 Garden Street
Cambridge, MA 02138
USA

[7]Space Science Center
University of New Hampshire
8 College Rd
Durham, NH 03824
USA

[8]Department of Space and Climate Physics
Mullard Space Science Laboratory
University College London
Holmbury St. Mary
Dorking
Surrey RH5 6NT
UK

[9]INAF-IFSI
Via del Fosso del Cavaliere 100
00133 Rome
Italy
[10]Institut de Recherche en Astrophysique et Planétologie
9 Avenue du Colonel ROCHE
BP 4346, 31028 Toulouse Cedex 4
France

Abstract. Charged particle acceleration and heating in the heliosphere requires detailed observations of the velocity distribution functions (VDFs) of these particles across a range of mass and charge states. Such particle energization is often observed concurrent with transient phenomena. Proper characterization of such energization processes and their impact on charged particles requires careful consideration of instrument observation timing and the timing at which a transient phenomenon is observed. Solar Orbiter's Heavy Ion Sensor (HIS) observes the composition of the solar wind along with suprathermal and pickup ions. As such, it provides the observations necessary to resolve the mass and charge states appropriate for properly characterizing charged particle energization. In this work, we describe the current status of data aggregation at variable time intervals and how that enables proper characterization of charged particle energization concurrent with transient phenomena.

Keywords. Interplanetary shocks (829), Solar coronal mass ejections (310)

---

1. Introduction

Transient phenomena such as shocks, coronal mass ejections (CMEs), and stream interaction regions (SIRs) are key drivers of heliospheric variability. In particular, they are known to heat and accelerate charged particles. Two of Solar Orbiter's four science objectives aim to understand transient phenomena in the heliosphere and the origin of energetic particles (Müller et al. 2013, 2020). Fully characterizing these phenomena requires high time resolution, statistically significant observations of charged particles across a wide range of energies from thermal solar wind energies up to energetic particles (Müller et al. 2013, 2020). The ability to resolve ion mass (M) and charge state (Q) is critical to such investigations because various theories of charged particle energization depend on these quantities and/or their charge-to-mass ratio (Q/M). Solar Orbiter's Heavy Ion Sensor (HIS) is a time-of-flight (ToF) mass spectrometer that provides the mass- and charge-resolved composition observations necessary to fully characterize transient phenomena, as listed in Solar Orbiter's science objectives (Müller et al. 2013, 2020; Owen et al. 2020; Livi et al. 2023).

In this paper, we provide a brief description of HIS, including its data products. We also demonstrate that HIS's high resolution observations can be aggregated in custom intervals that account for transient events. We then overview an interplanetary coronal mass ejection (ICME) driven shock observed by Solar Orbiter on March 11, 2022 and illustrate custom aggregation of HIS observations in a manner accounting for shock timing.

2. The Heavy Ion Sensor (HIS)

HIS is one of three instruments in the Solar Wind Analyzer (SWA) suite. HIS measures solar wind heavy, suprathermal, and pickup ions (PUI) over the energy-per-charge (E/Q) range $0.5 - 75\,\mathrm{keV/e}$. Owen et al. (2020); Livi et al. (2023) provide a detailed description of the instrument, its operational capabilities, and the first results. In addition to HIS, SWA is composed of the Electron Analyzer System (EAS) and the Proton-Alpha Sensor (PAS). Together, these three instruments make *in situ* observations of solar wind ions and electrons. Owen et al. (2020) describe the instrument suite along with all three instruments in detail.

HIS derives heritage from the Advanced Composition Explore (ACE) (Stone et al. 1998) Solar Wind Ion Composition Spectrometer (SWICS) (Gloeckler et al. 1998). Owen et al. (2020, Fig. 10) is a photo of the delivered instrument. Livi et al. (2023, Fig. 1) and Owen et al. (2020, Fig. 11) are schematics illustrating HIS's principle of operation.

HIS' Level 2 (L2) data include individual ion measurements, called pulse height analyzed (PHA) words. PHA words consist of the observed E/Q, residual energy, and time-of-flight (ToF) through the instrument of an ion observed at a given azimuth (ϕ) and elevation (θ) along with additional operationally determined and/or required quantities (Owen et al. 2020; Livi et al. 2023). Level 3 (L3) data is "science ready" and includes various products. The products of interest in this paper include ion speeds and temperatures. The method of converting PHAs to physical quantities for HIS data is comparable to that applied to ACE/SWICS (Livi et al. 2023; Shearer et al. 2014), which primarily focuses on data aggregation, ion species separation, and conversion to physical quantities. Livi et al. (2023) find a robust comparison between HIS composition data and corresponding ACE/SWICS observations. L2 and L3 HIS data are publicly available on the Solar Orbiter Archive (SOAR, `soar.esac.esa.int`)

2.1. *HIS Data*

HIS observes the solar wind from $-33°$ to $+66°$ in azimuthal (ϕ) and $\pm 17°$ in elevation (θ) bins (Owen et al. 2020). A single HIS scan consists of observing all relevant ϕ and θ across the full energy-per-charge range from 0.5 to 75 keV/e. HIS covers this energy-per-charge range by stepping its electrostatic analyzer from its 75 keV/e maximum down. While HIS is capable of observing solar wind H^{1+} at its lowest energy steps, HIS often avoids the energy range associated with H^{1+} to protect and prolong the lifetime of key hardware components. This is colloquially referred to as "proton avoidance".

Solar Orbiter observed a shock on March 11, 2022 at 19:52 UT (Dresing et al. 2024; Trotta et al. 2024). The shock is described in Section 3. Figure 1 is a plot of L2 HIS observations of E/Q as a function of ToF upstream and downstream of the shock. Both intervals are accumulated over 30 minutes to illustrate the changes across the shock. The purple region separated by a black dashed line indicates observations corresponding to spurious or accidental ToF signals. The plotted threshold corresponds to a speed $v < 0.7 \times v_{\mathrm{sw}}$, where v_{sw} is the solar wind speed, and we use it for illustrative purposes here. Livi et al. (2023) utilize $v_{\mathrm{sw}} - 2w$, where v_{sw} and w (the thermal speed) are both derived from O^{6+} observations. (E/Q,ToF) tracks are plotted for H^{1+}, He^{2+}, C^{6+}, and Fe^{8+} to Fe^{12+}. Numbers on the top axis indicate these ions charge states; only even Fe charge states are labeled for visual clarity. The centers and widths of these tracks are derived from ground calibration and comparison with in-flight data.

Figure 1 shows several key features of the HIS observations. In the downstream region, the shaded region corresponding to $v < 0.7 \times v_{\mathrm{sw}}$ covers a larger range of E/Q steps, corresponding to an increase in v_{sw} of $\sim 200\,\mathrm{km\,s^{-1}}$ across the shock (c.f. Figure 2). HIS steps from high to low E/Q. To protect the lifetime of certain instrument components, HIS implements a "proton avoidance", which does not step to certain low E/Q values during a given scan when the flux is high. The minimum E/Q reached varies with each scan. Here, we provide a brief overview of the effect. In upstream and downstream region, HIS's proton avoidance cut off portions of at least the H^{1+} and He^{2+} peaks. In the upstream region, this is less pronounced as the overall solar wind speed and flux are

https://doi.org/10.1017/S1743921324001790 Published online by Cambridge University Press

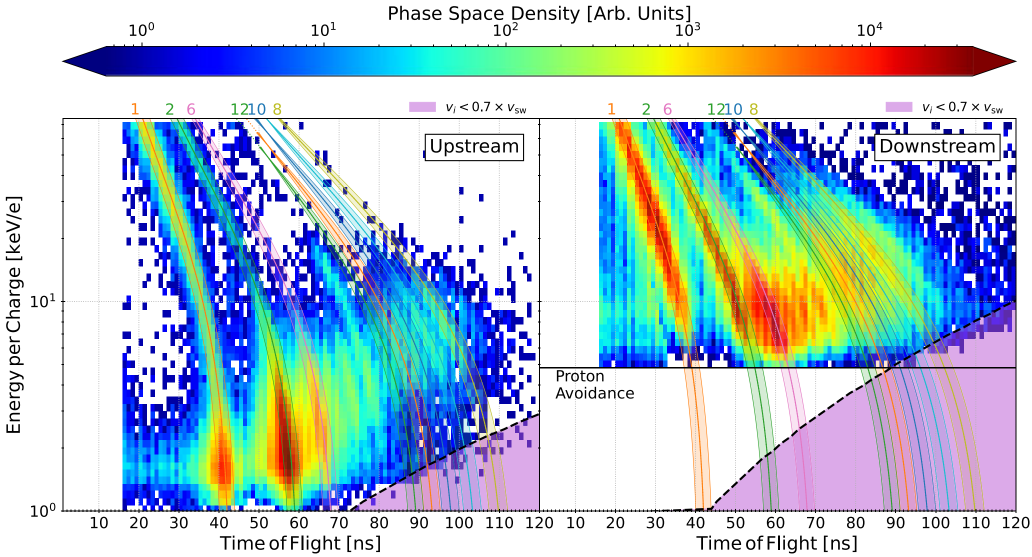

Figure 1. Energy-per-Charge (E/Q) vs Time-of-Flight (ToF) plots aggregated for 30 minutes upstream and downstream of the shock. (E/Q,ToF) tracks are plotted for H^{1+}, He^{2+}, C^{6+}, and Fe^{8+} to Fe^{12+}. Numbers on the top axis indicate these charge states; only even numbered Fe charge states are labeled for clarity. The region in the lower right corner of each plot covered by a purple region indicate where ToF accidentals occur, as determined by an ion having an incident speed $< 0.7 \times v_{\mathrm{H}}$.

smaller. In the downstream region, the flux is markedly higher and the C^{6+} peak is also cut off because HIS does not step to a larger range of voltages. We indicate this threshold in the downstream region as E/Q steps below the horizontal line at 4.82 keV/e. Livi et al. (2023) demonstrate proton avoidance in greater detail, including how it varies with each scan. As the bulk of Fe^{8+} to Fe^{12+} enter the instrument at E/Q steps above proton avoidance, their peaks are observed in both the upstream and downstream regions. The center of these Fe peaks is at higher E/Q in the downstream region and the extent of these distributions in (E/Q,ToF) space is also larger in the downstream region.

Similar to ACE/SWICS, HIS data processing utilizes a maximum likelihood estimator (MLE) to attribute count rates to specific ions based on the distribution in (E,ToF) space (Livi et al. 2023; Shearer et al. 2014). Livi et al. (2023, Fig. 2) illustrates the relationship between observations in (E/Q,ToF) space and (E,ToF) space and discusses the relevant aspects of the method. Although computationally expensive, this method separates ions with comparatively smaller count rates or that have overlapping distributions in measurement space Figure 1 (Shearer et al. 2014). Level 3 (L3) is considered "science" data, i.e. physical quantities useful for immediate data analysis. L3 quantities for each ion are derived by taking moments of the velocity distribution functions (VDFs) after they have been assigned to a given ion by MLE. **Such observations are typically plotted as the phase space density (PSD) as a function of E/Q.** HIS has two operational modes: normal and burst mode (Owen et al. 2020; Livi et al. 2023). L2 burst mode data is collected at 4s cadence and discussed in Owen et al. (2020); Livi et al. (2023). We use "normal mode" L2 data, which are collected at 30s cadence. Version 01 of the L3 data is distributed at 10min resolution due to instrumental considerations (Livi et al. 2023, Tbl. 2). As of this paper's writing, data in the SOAR covers the time period January 2022 to April 2023.

We have developed a preliminary version of the data processing software that enables variable time intervals to be selected for aggregating L2 observations. Figure 1 is

https://doi.org/10.1017/S1743921324001790 Published online by Cambridge University Press

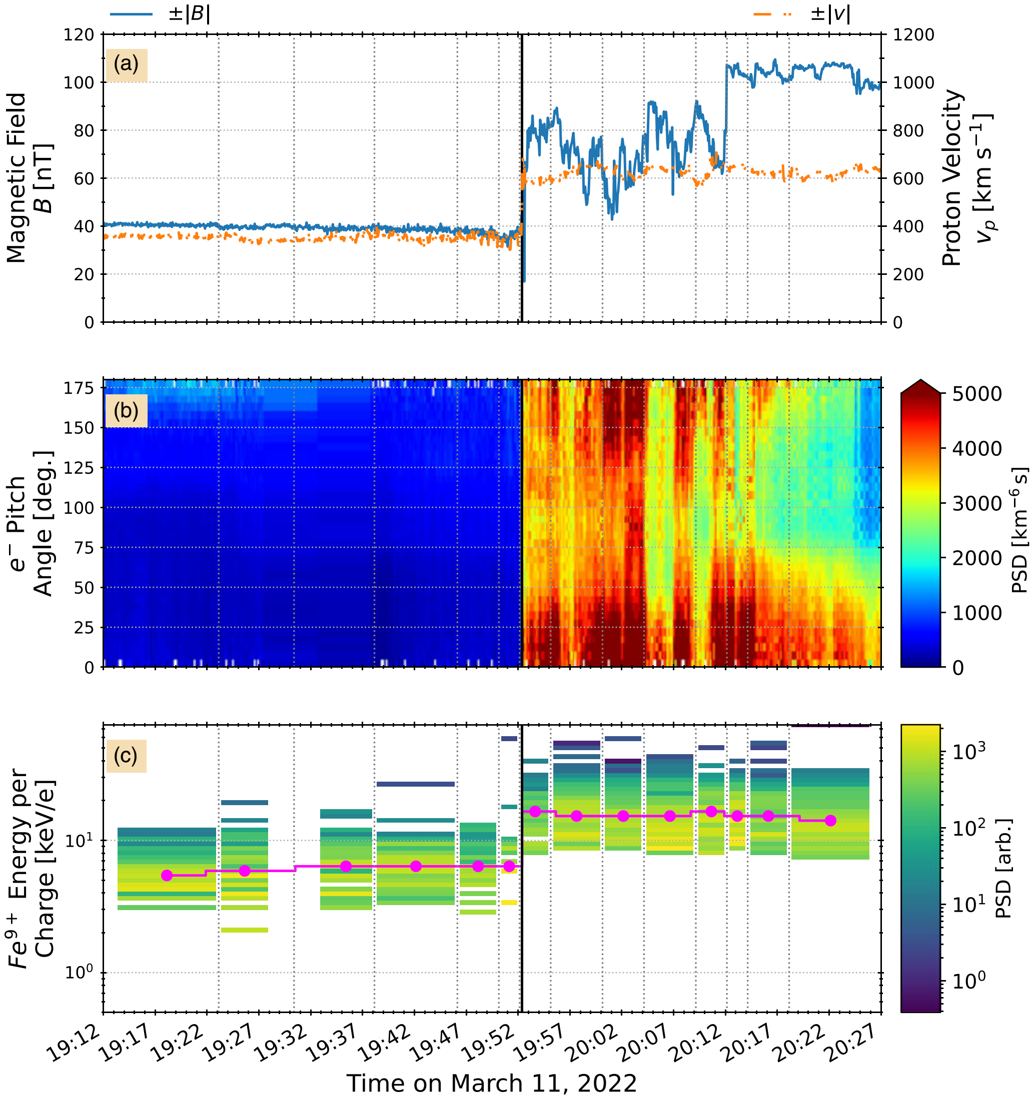

Figure 2. Overview of the event observed by HIS on March 11, 2022 at ∼19:52. Panels are **(a, left)** magnetic field magnitude from MAG, **(a, right)** proton speed from PAS, **(b)** electron pitch angle distribution from EAS, and **(c)** a spectrogram of Fe^{9+} aggregated to the indicated intervals. Gaps in panel (c) and vertical dotted lines indicate the variable width intervals in which HIS observations are aggregated. The vertical solid line at ∼19:52 indicates when SolO observed the shock.

aggregated into 30min intervals so that count rates are high and features in the observations are visually recognizable. In the following section, we show that observations can also be aggregated into intervals several minutes in length to enable studies of transient events that do not align with the 10min cadence of current L3 data.

3. March 11, 2022 Shock

On March 11, 2022 Solar Orbiter observed a shock at 0.44 AU while inbound towards the 1st science perihelion. This fast-forward shock was embedded in a interplanetary CME (ICME). The shock parameters are derived following Trotta et al. (2022). Briefly,

https://doi.org/10.1017/S1743921324001790 Published online by Cambridge University Press

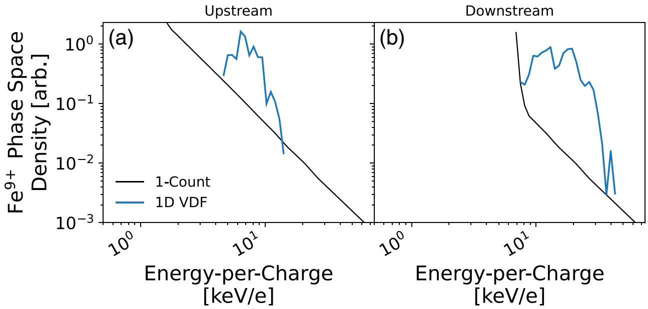

Figure 3. Fe^{9+} VDFs **plotted as the phase space density (PSD)** from the **(a)** upstream and **(b)** downstream region as a function of energy-per-charge. The upstream VDF is observed at 19:42. The downstream VDF is observed at 20:22. The 1-count levels are shown as black lines.

the shock normal angle is $\theta_{Bn} = 27°$; the Mach number is $M_A = 3.2$; and the shock speed is 737 km s^{-1} in the spacecraft frame (Dresing et al. 2024; Trotta et al. 2024).

Figure 2 provides a timeseries overview of the shock. Panel (a) plots (left) the magnetic field magnitude observed by MAG (Horbury et al. 2020) and (right) the proton speed observed by PAS (Owen et al. 2020). Panel (b) is an electron pitch angle distribution (PAD) from EAS (Owen et al. 2020). Panel (c) is a 1D spectrogram for Fe^{9+}, which means that PHA words are accumulated over both azimuth and elevation angles to improve overall statistics. Both the HIS and EAS spectrograms are plotted as a phase space density (PSD). The typical unit for a VDF is $\text{km}^{-6}\,\text{s}^3$. For this, deriving such units requires cross calibration with PAS, which is still being refined. As such, this Fe^{9+} spectrogram units are arbitrary. The spectrogram peaks are plotted with dots and connected to aid the eye. The time intervals are variable in length. The spectrogram gaps indicate 30s separation between adjacent accumulations. In contrast to the 30min intervals utilized in Figure 1 and the 10min cadence intervals used by Livi et al. (2023), these intervals range from ~ 2 to ~ 8 minutes. The gaps and vertical dotted lines indicate 30s intervals where PHA words are not utilized because either the start or end time did not fall into the specified accumulation interval. A vertical black line indicates the shock time at 19:52 UT.

There are multiple changes across the shock that can be observed in the data. Panel (a, left) shows that $\boldsymbol{B}$ is approximately constant and $|\boldsymbol{B}| \approx 40$ nT in the upstream region. In the downstream region, $|\boldsymbol{B}| \approx 80$ nT and is highly variable. In Panel (a, right), the proton velocity increases across the shock from ~ 350 to $\sim 580\,\text{km s}^{-1}$. In Panel (b), the electron PAD shows periods that are bi-directional and uni-directional with PSD spread that is wide in pitch-angle similar to shock sheath of ICMEs where it is likely the shock efficiently scatters electrons in pitch-angle (Carcaboso et al. 2020). As expected from Figure 1, the E/Q corresponding to the peak of the Fe spectrogram in Panel (c) increases markedly across the shock. The distribution also broadens in the downstream region.

Figure 3 is an example of Fe^{9+} VDFs from the (a) upstream and (b) downstream regions observed at 19:42 UT and 20:22 UT, respectively. Both are 7.5min in length. The upstream interval is chosen to be close to the shock. The downstream period is chosen to be far downstream. The units are arbitrary for the same reason that the HIS PSD in Figure 2 are. The black lines indicate the 1-count level in the upstream region. Although the lowest E/Q observation in the downstream region is close to the 1-count level, all higher E/Q observations are significantly above this level. Consistent with Figure 2, the upstream distribution peaks at ~ 6.5 keV/e; the downstream distribution

https://doi.org/10.1017/S1743921324001790 Published online by Cambridge University Press

peaks at $\sim 18\,\mathrm{keV/e}$; and the minimum E/Q at which Fe^{9+} is observed increases in the downstream region.

4. Results

Solar Orbiter's Heavy Ion Sensor provides high time resolution ion composition observations with both mass and charge state resolution. Currently available data has 10min time resolution. We have presented HIS observations from a shock observed by Solar Orbiter on March 11, 2022. The instrument's proton avoidance prevent a comparison of H^{1+}, He^{2+}, and O^{6+} across the shock. However, Fe^{8+} to Fe^{12+} are well resolved in both the upstream and downstream regions.

We have aggregated L2 PHA words collected in HIS' normal mode into variably defined intervals that range from ~ 2 to ~ 8 minutes. To improve statistics, PHAs have also been accumulated over azimuth and elevation angles. We show that the peak E/Q for Fe^{9+} increases across the shock. The VDFs derived from these spectra are above the 1-count level. Future, detailed analysis of multiple charge states is necessary to characterize the interaction between the observed heavy ions and the shock.

Further developments for HIS data are ongoing. Owen et al. (2020) describes the full complement of possible products. Several products under active development include expanded Fe charge states, high confidence derived physical quantities for an expanded set of elements and charge states, VDFs derived from onboard classification, and angular calibrations. Future cross-calibration with PAS will provide an absolute density calibration and intercalibration with the Suprathermal Ion Spectrograph (SIS) in the Energetic Particle Detector suite (EPD, Rodríguez-Pacheco et al. 2020; Wimmer-Schweingruber et al. 2021) will also provide observations of suprathermals across the energy ranges necessary to characterize multiple aspects of charged particle energization.

5. Acknowledgements

This work is funded by NASA contract NNG10EK25C.

References

Carcaboso, F., Gómez-Herrero, R., Espinosa Lara, F., et al. 2020, Astronomy & Astrophysics, 635, A79, doi: 10.1051/0004-6361/201936601

Dresing, N., Yli-Laurila, A., Valkila, S., et al. 2024, Astronomy & Astrophysics, 687, A72, doi: 10.1051/0004-6361/202449831

Gloeckler, G., Cain, J., Ipavich, F. M., et al. 1998, Space Sci. Rev., 86, 497, doi: 10.1023/A:1005036131689

Horbury, T. S., O'Brien, H., Carrasco Blazquez, I., et al. 2020, Astronomy & Astrophysics, 642, A9, doi: 10.1051/0004-6361/201937257

Livi, S., Lepri, S. T., Raines, J. M., et al. 2023, Astronomy & Astrophysics, 676, A36, doi: 10.1051/0004-6361/202346304

Müller, D., Marsden, R. G., St. Cyr, O. C., & Gilbert, H. R. 2013, Solar Physics, 285, 25, doi: 10.1007/s11207-012-0085-7

Müller, D., St. Cyr, O. C., Zouganelis, I., et al. 2020, Astronomy & Astrophysics, 642, A1, doi: 10.1051/0004-6361/202038467

Owen, C. J., Bruno, R., Livi, S. A., et al. 2020, Astronomy & Astrophysics, 642, A16, doi: 10.1051/0004-6361/201937259

Rodríguez-Pacheco, J., Wimmer-Schweingruber, R. F., Mason, G., et al. 2020, Astronomy & Astrophysics, 642, A7, doi: 10.1051/0004-6361/201935287

Shearer, P., von Steiger, R., Raines, J. M., et al. 2014, The Astrophysical Journal, 789, 60, doi: 10.1088/0004-637X/789/1/60

Stone, E. C., Frandsen, A. M., Mewaldt, R. A., et al. 1998, Space Science Reviews, 86, 1, doi: 10.1023/A:1005082526237

Trotta, D., Vuorinen, L., Hietala, H., et al. 2022, Frontiers in Astronomy and Space Sciences, 9, 1005672, doi: 10.3389/fspas.2022.1005672

Trotta, D., Hietala, H., Dresing, N., et al. 2024, Solar Orbiter Cycle 25 Interplanetary Shock List, Zenodo, doi: 10.5281/ZENODO.12518015

Wimmer-Schweingruber, R. F., Janitzek, N. P., Pacheco, D., et al. 2021, Astronomy & Astrophysics, 656, A22, doi: 10.1051/0004-6361/202140940